A FRAMEWORK OF CHANGE DETECTION BASED ON COMBINED MORPHOLOGICA FEATURES AND MULTI-INDEX CLASSIFICATION

Shuang Li [a], Shuming Zhang [a], Daiqin Yang [a, *]

[a] School of Remote Sensing and Information Envgineering, Wuhan University, 430079 Wuhan China - dqyang@whu.edu.cn

Commission III, WG III/6

KEY WORDS: Change detection, Multi-index, Morphological

ABSTRACT:

Remote sensing images are particularly well suited for analysis of land cover change. In this paper, we present a new framework for detection of changing land cover using satellite imagery. Morphological features and a multi-index are used to extract typical objects from the imagery, including vegetation, water, bare land, buildings, and roads. Our method, based on connected domains, is different from traditional methods; it uses image segmentation to extract morphological features, while the enhanced vegetation index (EVI), the differential water index (NDWI) are used to extract vegetation and water, and a fragmentation index is used to the correct extraction results of water. HSV transformation and threshold segmentation extract and remove the effects of shadows on extraction results. Change detection is performed on these results. One of the advantages of the proposed framework is that semantic information is extracted automatically using low-level morphological features and indexes. Another advantage is that the proposed method detects specific types of change without any training samples. A test on ZY-3 images demonstrates that our framework has a promising capability to detect change.

1. INTRODUCTION

With the development of satellite remote sensing technology, remote sensing imagery is easy to acquire, with ever wider fields of application. Remote sensing imagery has short imaging period, low cost and wide range. Multi-spectral remote sensing is a widely used data source and it is easy to obtain. Land cover / use change detection is an important application of remote sensing images, aiding urban planning, land management, and disaster monitoring. The problems addressed by change detection include determining whether a change has occurred, the location of the changed area and the type of change (Sun et al, 2011). The general steps in change detection are: data selection, data preprocessing, change information extraction and precision evaluation.

The method of change detection based on multi-spectral image can be divided into pixel based and object based. The pixel based method is performing difference or ratio processing on pixel-level features, then a threshold segmentation is used to extract change information.

Wang et al. (2011) normalized the pixels, and generated difference images and parameters by the linear combination method. The parameters were optimized by the Bayesian Optimization algorithm and the the change image was obtained.

MA et al. (2006) constructed the difference by combining difference and ratio operation, and then used the gray morphology to get the spatial neighborhood relationship of the difference image. The generalized Gaussian distribution model was used to estimate the probability density parameters of the change and non-changing pixels. An improved KI algorithm was used to calculate the optimal segmentation threshold and extract the change region.

Dian et al. (2009) used D-S (dempster-shafer) theory to combine multiple variation detection algorithms to form a fusion difference layer, and a binary decision was made to detect changes. These pixel based method only consider the single pixels and do not exploit the spectral characteristics of the surrounding pixels and neighboring pixels, and are sensitive to noise.

The object based methods divide the image into the objects composed of homogeneous pixels, and the features of the objects are extracted for comparison to detect changes (Wei et al, 2010, Wang et al, 2013). The disadvantage of these methods is that the existing segmentation algorithms have limitations, so it is difficult to achieve the best segmentation for the same class.

Machine learning methods are also applied in the change detection application. Bovolo et al. (2010) proposed a method for time series image change detection based on support vector machine and change vector analysis. Ashish et al. (2013) proposed a spatial context-based non-supervised change detection method based on a Hopfield neural network, using multi-temporal remote sensing image.

In this paper, we propose a change detection framework based on morphological features and multi-index classification, using multi-spectral images. A fragmentation index is defined to correct water extraction results. Using morphological operations combined with semantic information we extract bare land, roads and buildings. The extraction process is automatic and does not need any training samples. Change detection is performed using a land cover map based on extraction results. Our framework can not only detect changes, but also detects the type of change at the pixel level.

2. PROPOSED FRAMEWORK

The overall framework of the change detection is shown in Figure 1.

* Corresponding author

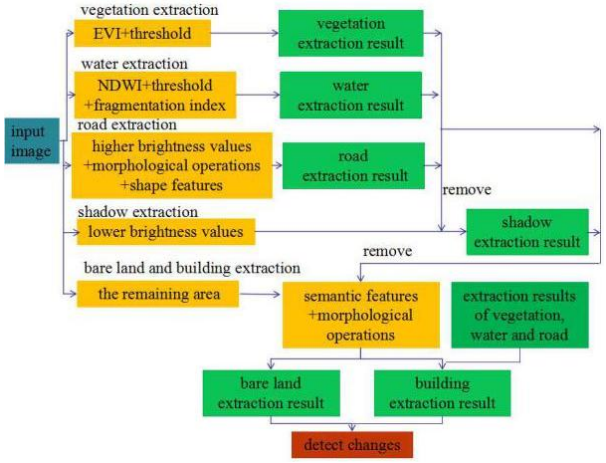

Figure 1. The proposed framework

2.1 Vegetation extraction

EVI (the enhanced vegetation index) adds a blue band based on the Normalized Vegetation Index (NVDI) to enhance the effects of vegetation signals and corrects soil background and aerosol scattering (Wang et al, 2003). EVI is commonly used when the leaf area index (leaf LAI) is high, with a dense vegetation area. The formula of EVI is:

$$EVI = 2.5\left(\frac{\rho_{NIR} - \rho_{RED}}{\rho_{NIR} + 6\rho_{RED} - 7.5\rho_{BLUE} + 1}\right) \quad (1)$$

where ρ_{NIR} = the reflectance in near-infrared band

ρ_{RED} = the reflectance in red band

ρ_{BLUE} = the reflectance in blue band

After calculating EVI, a threshold was obtained by the OSTU method to extract vegetation. An example of extraction results is shown in Figure 2.

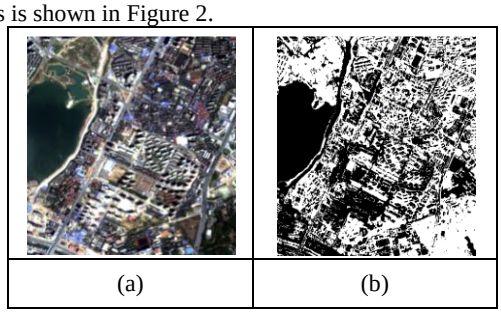

(a) (b)

Figure 2. Example of vegetation extraction result (a) original image; (b) vegetation extraction result

2.2 Water extraction

The normalized water index (NDWI) can be used to extract water covered areas using the difference between water reflectance in the green and near-infrared bands (McFEETERS et al, 1996). The definition of NDWI is as follows:

$$NDWI = \frac{\rho_{GREEN} - \rho_{NIR}}{\rho_{GREEN} + \rho_{NIR}} \quad (2)$$

where ρ_{NIR} = the reflectance in near-infrared band

ρ_{GREEN} = the reflectance in green band

These water extraction results however, are easily confused with shadows. Although NDWI can eliminate the influence of mountain shadows to a certain extent, it is not good for urban areas with more shadows. Figure 3 shows an example of shadows extracted as water.

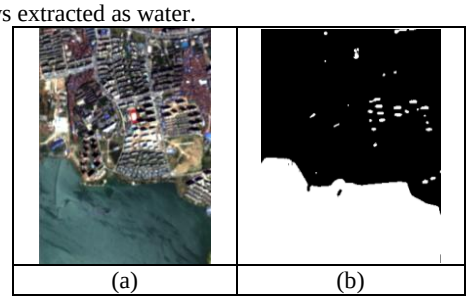

(a) (b)

Figure 3. An example of shadows extracted as water original image; (b) correct water extraction result and shadows extracted as water

A fragmentation index was defined to solve this problem. Water extraction results were binarized and divided into a regular grid. For binary water extraction results in every grid cell, similar connected cells, representing a domain were extracted. The number of domains with an area less than 1/n of the grid area was counted and denoted by numbersamll , and n was manually defined as 50. The total number of domains in that grid is denoted by numbertotal , and a fragmentation index was defined as follows to measure the degree of fragmentation in the grid area:

$$fragmentation\ index = \frac{number_{small}}{number_{total}} \quad (3)$$

where $number_{small}$ = the number of domains with an area less than 1/n of the grid area

$number_{total}$ = the total number of domains in the grid

Figure 4. A diagram of fragmentation index calculation

Figure 4 shows how to calculate the fragmentation index, domains with an area larger than 1/n of the grid area are represented as white, while domains with an area less than 1/n are represented as blue. It can be seen that numbertotal is 9 and numbersamll is 1, the value fragmentation index is 0.1.

The value of fragmentation index ranges from 0 to 1. Grids with fragmentation index value between m to 1 is a broken area, where m is a manually selected threshold whose value was 0.5. The upper limit of 1 is a case where there is only one small connected domain in a block, that is, an independent small lake. Then for the broken area, a connected domain with an area less than 1 / n (the value n is still 50) is considered shadow. Shadow removal results are shown in Figure 5.

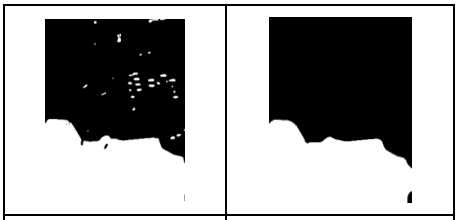

Figure 5. An example of shadow removal result (a) before shadow removal; (b) after shadow removal

The key parameters of the fragmentation index are n and m, which are used to describe the size of similar connected cells and measure the degree of fragmentation in an area respectively. The impacts of there two parameters on shadow removal are discussed as follows. The value of n varies from 10 to 90, while the value of m remains to be 0.5. The results are shown in Figure 6. Shadow removal results are not sensitive to value of n as long as it is in a suitable range. However, the value of n should not be too large. For example, shadows can not be completely removed when n is larger than 300 as shown in Figure 6. When m (the threshold of fragmentation index) varies from 0.1 to 0.9, the results are shown in Figure 7. It can be noticed that when the value of m is large, shadow removal results are effected.

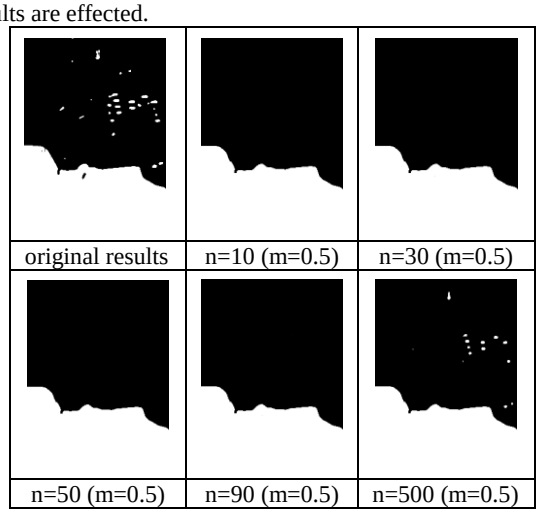

Figure 6. Shadow removal result with different values of n

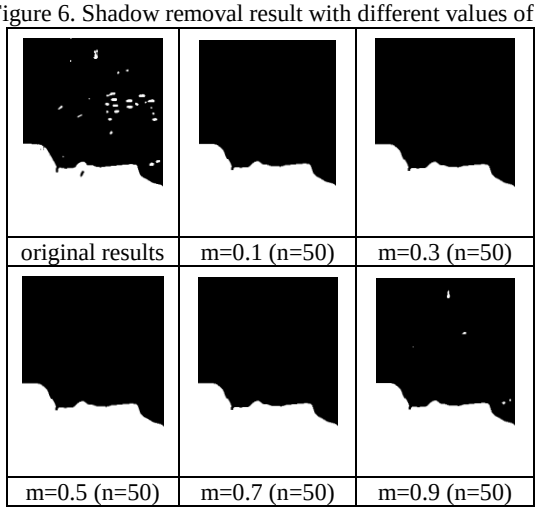

Figure 7. Shadow removal result with different values of m

2.3 Road extraction

An original image is binarized, and then a morphological opening and closing operation is used to process this image. HSV transform was performed on an original image to extract the area with higher brightness, where V is the value component, and the higher part of the V component is extracted. The threshold is chosen using the OSTU method. The initial road extraction results are obtained. Figure 8 shows an example of initial extraction result of an image.

Figure 8. An example of initial road extraction results from an image

The initial extraction result can be further modified by using the shape of the road; the initial extraction result is divided into regular grid and the connected domain was extracted. Grid segmentation aims to join domain extraction effect. The aspect ratio for the connected domain is calculated as:

$$Pwl = \frac{h}{w} \qquad (4)$$

where Pwl = aspect ratio

w = short side length of the minimum area bounding rectangle of a connected domain

h = long side length of the minimum area bounding rectangle of a connected domain

A diagram of minimum area bounding rectangle is shown in Figure 9. The aspect ratio of the road is relatively large and it is a shape feature of the road. For the initial extraction result, the domain whose aspect ratio of minimum area bounding rectangle is lager than a threshold is the road. The threshold was arbitrarily chosen as 10 in this example. An example is shown in Figure 10.

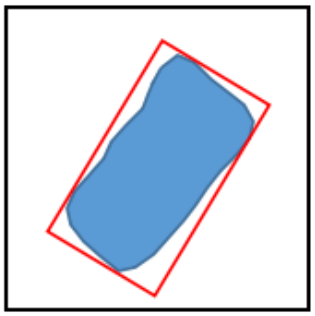

Figure 9. A diagram of minimum area bounding rectangle

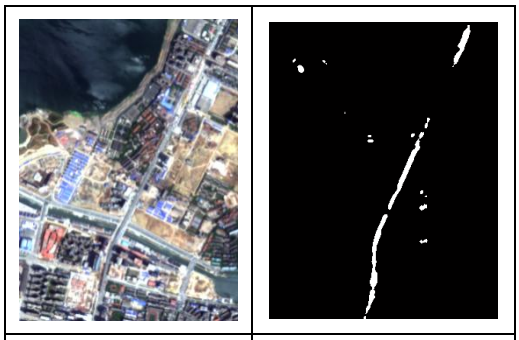

(a) (b)

Figure 10. An example of road extraction result (a) original image; (b) extraction result

2.4 Shadow extraction

Shadow can be extracted based on brightness. The RGB color space was converted into HSV color space, where V is the value component, and the lower part of the V component extracted as shadow. The threshold is the same as that in road extraction by the OSTU method. The extraction removed the vegetation, water, and road were from the shadow extraction results. An example of the shadow extraction results are shown in Figure 11.

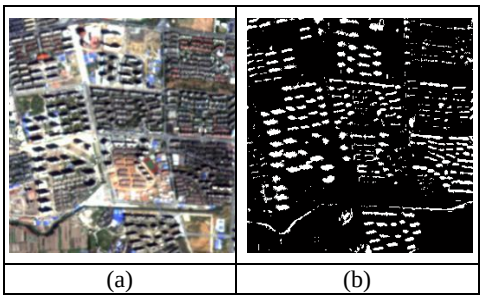

(a) (b)

Figure 11. An example of shadow extraction results (a) original image; (b) extraction result

2.5 Building and bare land extraction

After the extraction of vegetation, water, roads, and shadows, the remaining objects to be extracted were buildings and bare land. Bare land does not produce shadows, while buildings do produce them. The semantic information provided by the shadow around buildings can distinguish bare land and buildings.

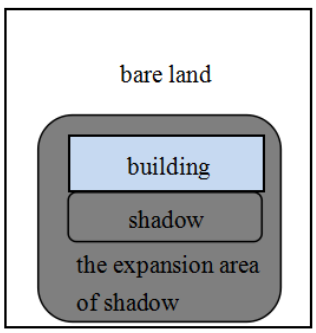

Figure 12. A diagram of the method for distinguishing bare land and buildings

As shown in Figure 12, after performing morphological expansion on the area of shadow with a cross-shaped SE (structure element), buildings were included in the expansion area. The size of cross-shaped SE was chosen as 3 considering the size of most buildings and the spatial resolution of images. Since the remaining area only contains bare land and buildings, only buildings were included in the expansion area of shadow. As Figure 13 (b) shows, the blue area is the expansion area of shadow, and the white areas are extracted buildings.

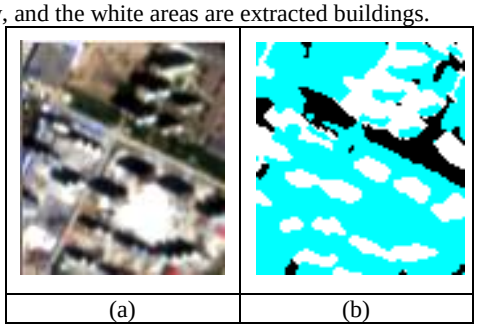

(a) (b)

Figure 13. An example of building extraction result (a) original image; (b) building extraction result

The impact of larger SE on building extraction results is explored as follows. Figure 14 shows the results using SE of different sizes. When using lager structural elements, non-buildings will appear in the building extraction results, especially when buildings are dense.

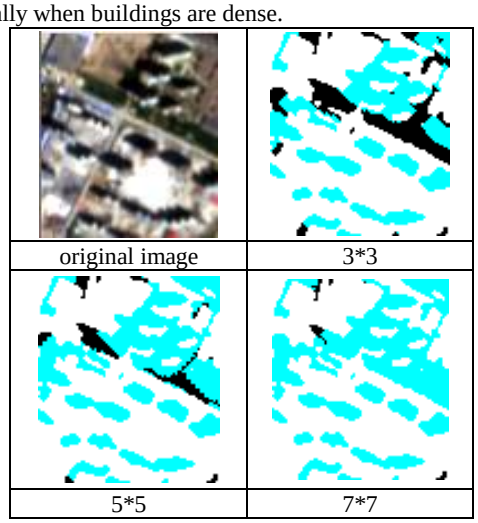

original image 3*3

5*5 7*7

Figure 14. Examples of building extraction results with structure elements of different sizes

2.6 Change detection

The land use map was obtained after the extraction of five typical objects (vegetation, water, buildings, roads, and bare land). However, our method is implemented by means of a series of low dimensional indexes and morphological operations, and no training sample was used. Examples of changed and unchanged areas are shown in Figure 15 and Figure 16 respectively. From Figure 15 (c)(d), it can be seen that two small water bodies change into vegetation in 2013, and some bare lands also change into vegetation. As shown,our method not only detects the changed areas, but also the specific type of change.

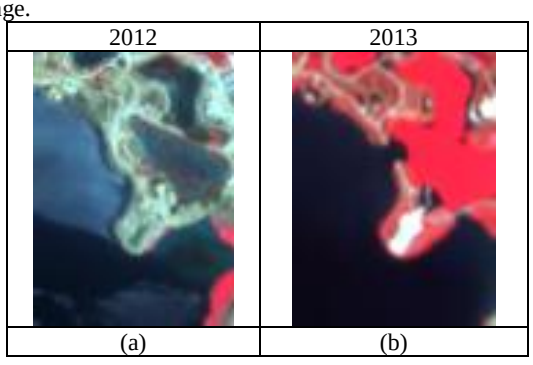

(a) (b)

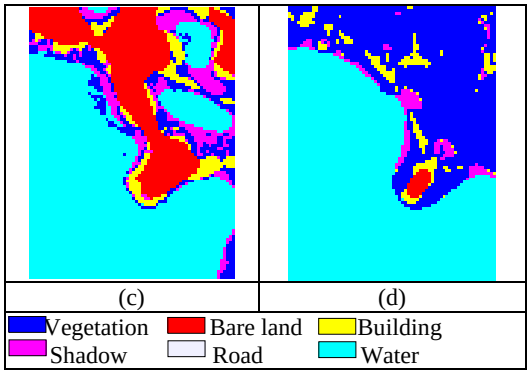

Figure 15. An example of changed area (a) (b) original image; (c) (d) extraction results in changed area

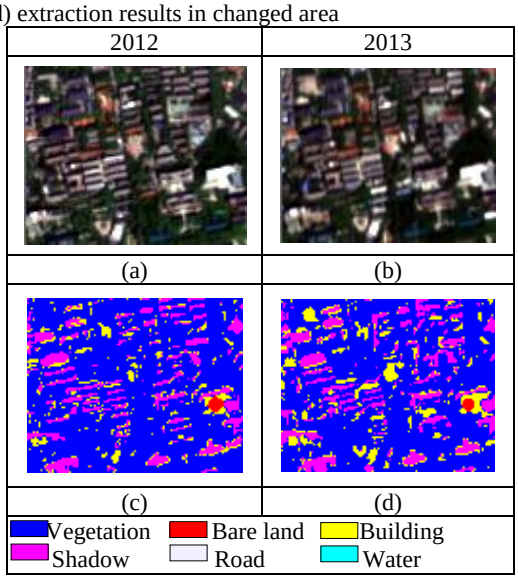

Figure 16. An example of unchanged area (a) (b) original image; (c) (d) extraction results in unchanged area

3. RESULTS

3.1 Data sets

The images used in this study are ZY-3 satellite images with four multi-spectral bands with 5.8 m spatial resolution. The study area is a part of Wuhan, a big city in China experiencing rapid development. The bitemporal images used were obtained on April 22, 2012 and August 12, 2013 as Figure 17 shows.

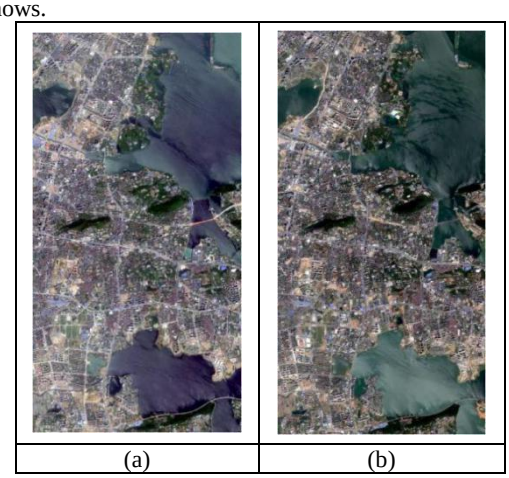

Figure 17. The bitemporal images (a) The image of 2012; (b)The image of 2013

3.2 Results of change detection

Figure 18 shows the extraction results of five typical objects (vegetation, water, building, roads, and bare land). The extraction of the shadow will aid the extraction of other objects.

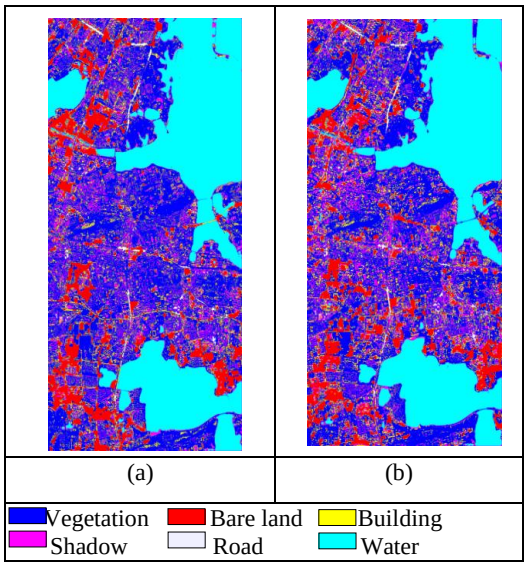

Figure 18. The extraction results of the five typical objects (a)2012; (b)2013

Figure 19 (a) shows binary change detection results. The accuracy evaluation of the change detection was done by visually selecting samples of the changed and unchanged areas. The confusion matrix is shown in Table 1. The overall accuracy is 0.94 and the kappa coefficient is 0.89. In addition, changes in each object were detected (Figure 19 (b)).

Confusion Matrix	changed	unchanged	
changed	1363	17	0.99
unchanged	150	1485	0.91
	0.97	0.99	0.94

Table 1. The confusion matrix

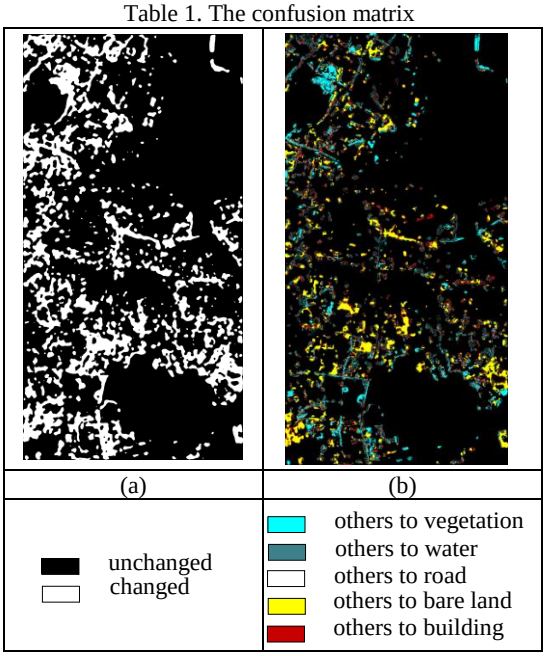

Figure 19. Change detection results (a) Binary change detection result; (b) Changes in each object

The change detection results provide more useful information. As Figure 20 shows, (a) (b) are false color images of the part of the study area in 2012 and 2013. The bright yellow area shown in Figure 20 (a) indicates that the area changed into bare land in 2013, the bright green area in Figure 20 (a) is an example of part of a lake changed into vegetation in 2013.

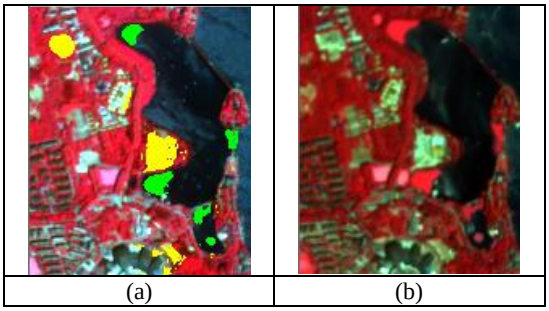

(a) (b)

Figure 20. Examples of information provided by the changed detection results

4. CONCLUSIONS

Our proposed framework using a multi-index combined with morphological operations and semantic features to extract the five typical objects (vegetation, water, buildings, roads, and bare land). A land cover map was obtained based on extraction results. Change detection was performed and changes in different objects were obtained, provide more useful information. The index and features used were low dimensional without complex calculations and training samples.

ACKNOWLEDGEMENTS

The authors would like to thank NASG (Satellite Surveying and Mapping Application Center) for providing the ZY-3 data set. The authors are also grateful for the language suggestions from Mr. Stephen C. McClure from the State Key Laboratory of Information Engineering in Surveying, Mapping and Remote Sensing.

REFERENCES

Bovolo, F., Camps-Valls, G., & Bruzzone, L., 2010. A support vector domain method for change detection in multitemporal images. *Pattern Recognition Letters*, 31(10), 1148-1154.

Dian, Y., & Fang, S., 2009. The change detection of multi-temporal remote sensing images based on d-s algorithm. *Proceedings of SPIE - The International Society for Optical Engineering*, 7492(3), 749224-749224-8.

Ghosh, A., Subudhi, B. N., & Bruzzone, L., 2013. Integration of gibbs markov random field and hopfield-type neural networks for unsupervised change detection in remotely sensed multitemporal images. *IEEE Transactions on Image Processing*, 22 (8), 3087-3096.

Guo-Rui, M. A., Ping-Xiang, L. I., & Qin, Q. Q., 2006. Based on fusion and ggm change detection approach of remote sensing images. *Journal of Remote Sensing*, 10(6), 847-853.

Luo, W., & Li, H., 2011. Soft-change detection in optical satellite images. *IEEE Geoscience & Remote Sensing Letters*, 8(5), 879-883.

S. K. McFEETERS., 2012. The use of the normalized difference water index (ndwi) in the delineation of open water features. *International Journal of Remote Sensing*, 17(7), 1425-1432

Sun, X. X., Zhang, J. X., Yan, Q., & Gao, J. X., 2011. A summary on current techniques and prospects of remote sensing change detection. *Remote Sensing Information*, 30(1), 119-123.

Wei, L., Li, P., Zhang, L., & Zhong, Y., 2010. An advanced change detection method based on object-oriented classification of multi-band remote sensing image. *International Conference on Geoinformatics* (pp.1-6). IEEE.

Wang, W. J., Zhao, Z. M., & Zhu, H. Q., 2009. Object-oriented multi-feature fusion change detection method for high resolution remote sensing image. *International Conference on Geoinformatics* (pp.1-6). IEEE.

Wang, X., 2013. Object-oriented change detection approach for high-resolution remote sensing images based on multiscale fusion. *Journal of Applied Remote Sensing*, 7(1), 073696.

Yang, C., Shen, R., Dawei, Y. U., Liu, R., & Chen, J., 2013. Forest disturbance monitoring based on the time-series trajectory of remote sensing index. *Journal of Remote Sensing*, 17(5), 1246-1263.